ReMo3D – an open-source Python package for 2D and 3D simulation of normal and lateral resistivity logs

Michał Wilkosz

AGH University of Science and Technology, Faculty of Geology, Geophysics and Environmental Protection,
Department of Geophysics, Krakow, Poland, e-mail: mwilkosz@agh.edu.pl, ORCID ID: 0000-0002-5146-0600

Abstract: An open-source Python package is presented, ReMo3D, which allows the generation of synthetic normal and lateral resistivity logs for 2D and 3D models. The package is built around a finite element mesh generator Gmsh and a high-performance multiphysics finite element software Netgen/NGSolve and supports distributed-memory parallel computation. The examples included in the paper show that the developed software can accurately simulate the measurement process and produce detailed synthetic normal and lateral resistivity logs. In addition, basic information about normal and lateral tools such as tool configurations, measurement principles, nomenclature and a brief history of utilization is included in the paper.

Keywords: normal and lateral resistivity logs, geophysical forward problem, finite element method, Python, Gmsh, Netgen/NGSolve

INTRODUCTION

The resistivity of a given rock formation is one of the most important parameters that can be measured during well logging. Normal and lateral logging tools were the first tools used to measure the resistivity of rock formations around boreholes. Throughout the years these tools have been extensively used in hydrocarbon prospection, mineral exploration, and hydrogeological, geotechnical and environmental surveys (Keys 1970, 1990, Keys & MacCary 1971, Allaud & Martin 1977, IAEA 2001, Asquith & Krygowski 2004, Acworth 2019). Therefore, many boreholes exist in which normal and lateral logs are the primary or sole source of information available about formation resistivity. Data from these boreholes are a very valuable and unique source of information that can be utilized

in current and future studies. However, the resolution and quality of normal and lateral resistivity logs are not on par with resistivity logs measured by modern, more advanced logging tools.

Numerical modelling plays a key role in modern interpretation techniques, such as iterative inversion and machine learning. The utilization of those techniques allows to bring logs measured by older, less sophisticated tools (such as normal and lateral logging tools) closer to modern standards. The modelling and inversion of normal and lateral resistivity logs have been extensively studied in the past (Yang & Ward 1984, Yuratich & Meger 1984, Towle et al. 1988, Whitman et al. 1989, 1990, Imamura & Shima 1991, Imamura 1992, Bittar et al. 1995, Frenkel et al. 1997, Yang & Shi 1999, Frenkel 2003, Nam et al. 2010, Ulugergerli 2011, Galsa et al. 2016, Glinskikh et al. 2017, Karataş

et al. 2019), but no software was provided together with those papers.

The main objective of the paper is to give the scientific community an open-source toolkit that allows for modelling normal and lateral resistivity logs and can be utilized to generate training datasets for machine learning algorithms or directly integrated into iterative inversion algorithms. The code provided alongside this paper is written in Python and is built around a finite element mesh generator Gmsh (Geuzaine & Remacle 2009) and a high-performance multiphysics finite element software Netgen/NGSolve (Schöberl 1997, 2014). It allows the simulation of normal and lateral resistivity logs in 2D and 3D formation models and supports distributed-memory parallel computation. In addition, basic information about normal and lateral resistivity logs such as tool configurations, measurement principles, nomenclature and a brief history of utilization is presented.

METHODS

Normal and lateral resistivity logging tools

Normal and lateral tools belong to the family of multi-electrode resistivity logging tools and are among the oldest logging tools to have been developed.

Tool configurations and measurement principles

Normal and lateral logging tools consists of two circuits – the current circuit and the measuring one. By convention, current electrodes are designated A and B, and potential electrodes are designated M and N. Three electrodes are located relatively close to each other and the fourth is placed far from them, in an effective infinity. In the normal tool configuration, the two closest electrodes are parts of different circuits. The tool spacing is equal to the distance between the two closest electrodes. In the lateral tool configuration, the two closest electrodes are parts of the same circuit. The tool spacing is equal to the distance between the measurement point and the further electrode. Generally speaking, the increase of tool spacing increases the depth of investigation

and reduces the vertical resolution of the tool. Therefore, logging tools with longer spacings are less affected by the borehole and filtration zone, and more affected by shoulder beds than their shorter counterparts (Serra 1984, Vincent & Williams 1995).

Normal and lateral tools can both exist in several different configurations depending on the number of current electrodes present in the tool assembly and the localization of two electrodes from the same circuit in relation to the third one (Fig. 1). In the single-electrode tool configuration, one current electrode and two measuring electrodes are located downhole while in the two-electrode tool configuration two current electrodes and one measuring electrode are located downhole. In the inverted/top tool configuration electrodes from the same circuit are located above the third one while in the standard/bottom tool configuration electrodes from the same circuit are located below the third one. In normal tools of Western design, a single measuring electrode can also be located between two current electrodes (Tittman 1986, Vincent & Williams 1995).

The electrodes are arranged in such a way that the measured parameter is the electric potential in the case of normal tools, and the difference of the electric potential in the case of lateral tools. The value of the measured apparent resistivity is given by the equation:

$$R_a = K \frac{V_M}{I} \tag{1}$$

in the case of a two-electrode tool configuration and by the equation:

$$R_a = K \frac{V_M - V_N}{I} \tag{2}$$

in the case of a single-electrode tool configuration, where K is a tool geometric factor, V_M and V_N are values of electric potential measured respectively by M and N electrodes, and I is the injected current. Calculated apparent resistivity is assigned to the depth of the logging tool measurement point which is located halfway between the two closest electrodes (Serra 1984).

Fig. 1. Different configurations of normal and lateral resistivity logging tools

History of utilization

The lateral logging tool was the very first tool to be developed and was first run on September 5, 1927, in a borehole in the Pechelbronn Field of France. The initial tests were followed by almost immediate commercial applications all over the world (Allaud & Martin 1977).

Initially, a single lateral tool was run to characterize the resistivity of the rock formation around the borehole. In 1932 a normal tool was developed and largely replaced the lateral tools, except for in the Soviet Union, where lateral tools with a spacing between 7.5 and 12 feet were kept in favor of normal tools and run alongside a self-potential (SP) log. In other parts of the world, a single normal tool was run alongside the SP log to characterize the resistivity of the rock formation around the borehole. The spacing of the tool was set in each region after a few tests and varied between 10 and 20 inches. In addition, the lateral tool with spacing between 12 and 24 feet was sometimes used in regions where more consolidated producing zones with deeper mud filtration zones occur. Utilization of the lateral tool alongside the normal one became the standard procedure around 1937. By the end of 1938, a second normal tool was added and electrode spacings were standardized. Since then, the standard resistivity logging suite utilized in hydrocarbon prospection in Western countries consisted of the short normal (16-inch), the long normal (64-inch) and the lateral tool (18 feet 8 inches) run alongside the SP log, although other spacings were also available. With the advent of laterologs and induction tools, the use of normal and lateral logging tools in the hydrocarbon prospecting industry diminished in Western countries between 1955 and 1965 (Allaud & Martin 1977).

The utilization of well logs in the Soviet Union and other countries of the Eastern Bloc differs significantly from concepts known in the West. Here, the idea of characterizing the resistivity of the rock formation around the borehole using multiple normal and lateral tools with a wide range of electrode spacing was implemented (Alpin 1938, Dakhnov 1941). The two most popular sets used in the hydrocarbon prospecting industry consisted of (1) five lateral logs and (2) two lateral logs and two normal logs each characterized by different spacing and run alongside the SP log.

However, boreholes, where significantly larger resistivity logging suites were run, can also be encountered. Laterologs and induction tools were known and utilized in those countries, but contrary to the Western countries normal and lateral tools were kept in favor and extensively used in the hydrocarbon prospecting industry until the 1990s when they started to be replaced by logging tools of Western design (Wiltgen & Truman 1993, Wiltgen 1994, Jakubowicz 1995, Tingey et al. 1995, Vincent & Williams 1995).

Normal and lateral logging tools remained in use in hydrogeological, geotechnical and environmental surveys as part of a standard and slim hole logging suites. Over the years, a variety of tool configurations were utilized in those applications. Most popular suites utilized in the West consist of (1) the short normal (16-inch) and the long normal (64-inch) tools, (2) the short normal (16-inch), the long normal (64-inch) and the lateral (18 feet 8 inches) tools, and (3) 8-, 16-, 32- and 64-inch normal tools, however different normal tools with spacing ranging from 8 to 84 inches and lateral tools with spacing ranging from 4 to 24 feet were also in use (Keys 1970, 1990, Keys & MacCary 1971, Acworth 2019). In the Soviet Union and other countries of the Eastern Bloc, tool configurations and interpretation techniques known from the hydrocarbon prospecting industry were utilized in those applications (Ogilvy 1970).

Nomenclature

There are three distinctive naming schemes of normal and lateral logging tools that can be encountered in the literature and borehole datasets.

Normal and lateral tools of Western design are usually referenced by the name and the spacing (e.g. short normal (16-inch), lateral (18 feet 8 inches)). In addition, a variety of mnemonics are used to specify those logs (e.g., R16, SN, or RESS for short normal, R64, LN, or RESD for long normal and R18, LT, or RLAT for lateral log).

In the Soviet Union and other countries of the Eastern Bloc, normal and lateral logging tools were characterized by symbols of three downhole electrodes listed from the top of the tool and separated by two numbers that specify distances between them in meters (e.g., A4.0M0.5N, M2.0N0.5A) (Jakubowicz 1995, Vincent & Williams 1995).

The third nomenclature was developed after Western logging companies encountered the Russian style logs to adjust their naming scheme to the requirements of the Western digital Log Information Standard (LIS) format which has a limit of four alphanumeric characters for curve mnemonics. The codes given to normal and lateral logs consists of one or two letters that specify tool type (N or EN for normal and L or EL for lateral log) and digits that fill remaining places and specify the spacing of a tool. If one letter and three digits are present in the code, the spacing is given in centimeters. If two letters and two digits are present within the code, the spacing is given in inches in the case of normal tools and feet in the case of lateral tools. In the case of direct/top tool configuration, the letters are followed by the number (e.g., EL04, EN16, L045) while in the case of inverted/bottom tool configuration the number is put in front of the single letter or inserted between the letters (e.g., E04L, E16N, 045L) (Jakubowicz 1995, Vincent & Williams 1995).

It is worth noting that each tool configuration is fully characterized by a distinctive name in the Eastern nomenclature while the other nomenclatures do not describe tool configuration fully and in a unique way (Tab. 1).

Table 1

Comparison of descriptions of selected normal and lateral tool configurations in different nomenclatures

Eastern	Western	Western descriptive
A2.0M0.5N	EL07 / L225	lateral (7 feet)
M2.0A0.5B	EL07 / L225	lateral (7 feet)
M0.5N2.0A	E07L / 225L	lateral (7 feet)
A0.5B2.0M	E07L / 225L	lateral (7 feet)
M2.0N0.5A	EN20 / 050N	normal (20 inches)
M6.0N0.5A	EN20 / 050N	normal (20 inches)
M8.0N0.5A	EN20 / 050N	normal (20 inches)
A0.5M2.0N	E20N / 050N	normal (20 inches)
A0.5M6.0N	E20N / 050N	normal (20 inches)
A0.5M8.0N	E20N / 050N	normal (20 inches)

Forward problem

The boundary value problem of 2D axisymmetric DC resistivity problem with a point source of electric current located at position $(0, z_s)$ is given

by the following equation of continuity with Neumann and Dirichlet boundary conditions:

$$\frac{1}{r}\frac{\partial}{\partial r}\left[r\sigma(r,z)\frac{\partial V(r,z)}{\partial r}\right]+\frac{\partial}{\partial z}\left[\sigma(r,z)\frac{\partial V(r,z)}{\partial z}\right]=$$

$$=-\frac{I\delta(r)\delta(z-z_S)}{2\pi r}\ \text{in}\ \Omega$$

$$\frac{\partial V(r,z)}{\partial r}=0\ \text{on}\ \Gamma_A \tag{3}$$

$$V(r,z)=0\ \text{on}\ \Gamma_E$$

where σ is a given conductivity distribution, V is the electrical potential, I is the current emitted from the electrode and δ is a Dirac's delta function.

The simulation domain is centered around the current electrode in the case of a single-electrode tool configuration or around the halfway point between current electrodes in the case of a two-electrode tool configuration. At the borehole axis Γ_A, the Neumann boundary condition is applied to impose symmetry of the model across the axis. The other external boundaries Γ_E are treated with the Dirichlet boundary condition (Fig. 2A).

The boundary value problem of 3D DC resistivity problem with a point source of electric current located at position $(0, 0, z_s)$ is given by the following equation of continuity with Neumann and Dirichlet boundary conditions:

$$\frac{\partial}{\partial x}\left[\sigma(x,y,z)\frac{\partial V(x,y,z)}{\partial x}\right]+\frac{\partial}{\partial y}\left[\sigma(x,y,z)\frac{\partial V(x,y,z)}{\partial y}\right]+$$

$$+\frac{\partial}{\partial z}\left[\sigma(x,y,z)\frac{\partial V(x,y,z)}{\partial z}\right]=-I\delta(x)\delta(y)\delta(z-z_S)\ \text{in}\ \Omega$$

$$\frac{\partial V(x,y,z)}{\partial x}=0\ \text{on}\ \Gamma_A \tag{4}$$
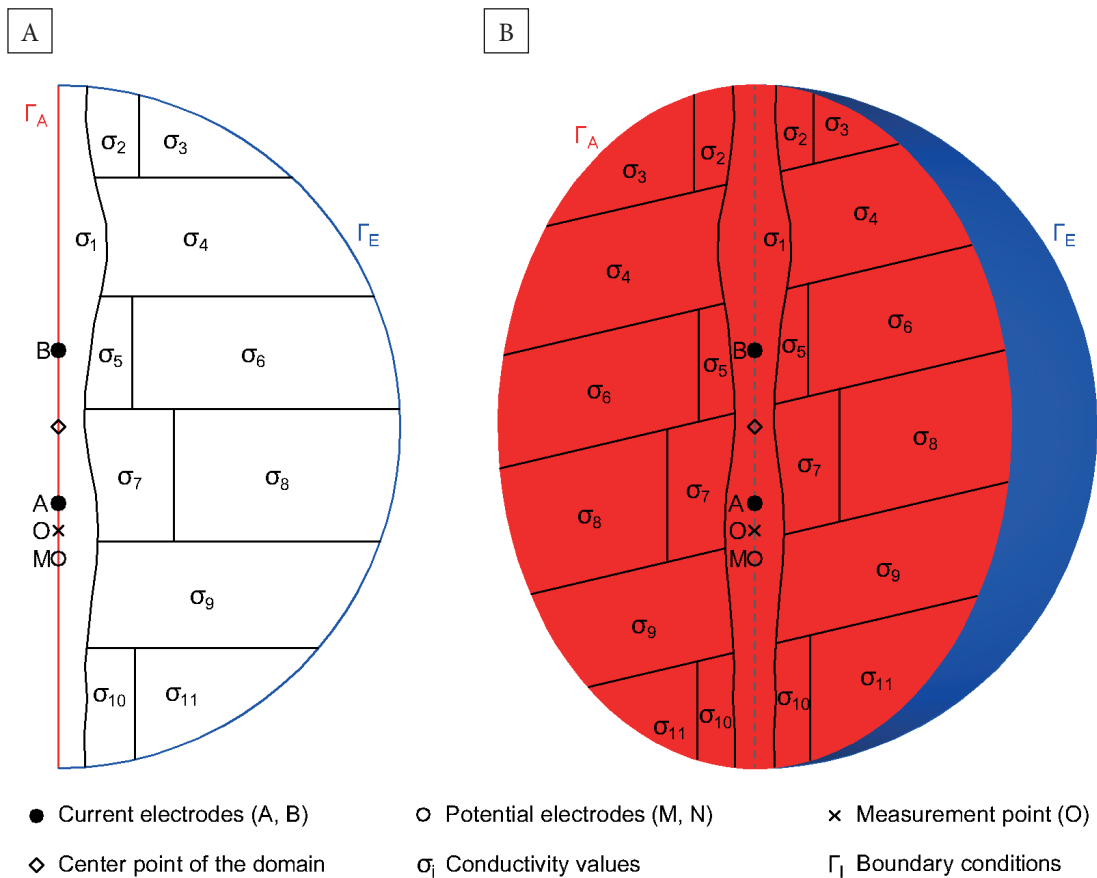
$$V(x,y,z)=0\ \text{on}\ \Gamma_E$$

Fig. 2. An illustration of (A) the 2D model and (B) the 3D model including the electrode configuration, the conductivity distribution within the model, the boundary conditions and the center point of the simulation domain

Similarly to the 2D model, the simulation domain is centered around the current electrode in the case of a single-electrode tool configuration or around the halfway point between current electrodes in the case of a two-electrode tool configuration. The 3D model geometry considered within the paper assumes that all layers are dipping in the same direction and under the same angle. Such a model is symmetric across the plane that contains the axis of the borehole and is parallel to the direction of the dip. Therefore, the model can be restricted to only one half of the sphere. The Neumann boundary condition is applied at the symmetry plane Γ_A to impose symmetry of the model across the plane. The other external boundaries Γ_E

are treated with the Dirichlet boundary condition (Fig. 2B). The value of the electric potential at the location of the measuring electrodes is retrieved from the model and used to calculate the value of measured apparent resistivity according to equation (1) or (2) depending on the configuration of the simulated logging tool. The calculated resistivity value is assigned to the depth at which the measurement point is located.

Application

The finite element method was selected to solve the forward problem described above, as it is naturally capable of handling complex geometries and boundary conditions.

```python
import remo3d as rm

import numpy as np


# Specify input data

tools = ["B5.7A0.4M", "B4.48A1.62M", "M1.0A0.1B", "A2.0M0.5N"]

formation_model_file = "./INPUT/FORMATION.txt"

borehole_model_file = "./INPUT/BOREHOLE.txt

measurement_depths = np.arange(0, 25.1, 0.1)


# Set tools parameters

tools_parameters = rm.SetToolsParameters(tools)


# Set model parameters

model_parameters = rm.SetModelParameters(formation_model_file,

        borehole_model_file, dip=30)


# Compute synthetic logs

logs = rm.ComputeSyntheticLogs(tools_parameters, model_parameters,

        measurement_depths, domain_radius=50, processes=12)


# Save results

output_folder = "./OUTPUT"

rm.SaveResults(model_parameters, measurement_depths, logs, output_folder)
```

Fig. 3. *A sample code that allows to generate a suite of synthetic normal and lateral resistivity logs for a given model*

The ReMo3D package is written in Python and built around a finite element mesh generator Gmsh (Geuzaine & Remacle 2009) and a high-performance multiphysics finite element software Netgen/NGSolve (Schöberl 1997, 2014). The package is built with MPI support through mpi4py (Dalcin et al. 2005, 2008, 2011, Dalcin & Fang 2021) and supports distributed-memory parallel computation with up to $n_{mp} \cdot n_t + 1$ processes, where n_{mp} is a number of measurement points and n_t is a number of simulated logging tools. The sample code is shown in Figure 3. The input data consists of a list of simulated logging tools in the Eastern nomenclature, the depths of measurement points, formation model parameters and borehole model parameters. In the example, both borehole and formation model data are imported from text files (Figs. 4, 5). However, they can also be easily created and manipulated entirely within the Python code if necessary.

DTOP	DBTM	RDFZ	RTFZ	RTUZ
M	M	M	OHMM	OHMM
0.00	2.05	1.00	4.00	10.00
2.05	5.05	NaN	NaN	3.00
5.05	9.05	0.50	4.00	15.00
...				
22.00	23.00	NaN	NaN	15.00
23.00	23.95	2.00	5.00	7.50
23.95	25.00	NaN	NaN	2.50

Fig. 4. *The formation model file consists of five columns: DTOP – depths at which tops of layers are located, DBTM – depths at which bottoms of layers are located, RDFZ – radii of filtration zones, RTFZ – values of resistivity within filtration zones, and RTUZ – values of resistivity within undisturbed zones. The file begins with the header where mnemonics and units are presented. The NaN values are used in layers without a filtration zone. In the figure, some rows are omitted for the sake of maintaining visual clarity and keeping a reasonable image size*

DEPT	CALI	RMUD
M	M	OHMM
0.00	0.236	1.1000
0.10	0.244	1.1002
0.20	0.246	1.1004
...		
24.80	0.264	1. 1496
24.90	0.266	1.1498
25.00	0.267	1.1500

Fig. 5. *The borehole model file consists of three columns: DEPT – depth, CALI – borehole diameter or radius, and RMUD – resistivity of the drilling mud. The file begins with the header where mnemonics and units are presented. In the figure, some rows are omitted for the sake of maintaining visual clarity and a reasonable image size*

The modelling process is carried out independently for each tool and for each depth at which a measurement was taken. The process starts with selecting data relevant to building a model for a given tool, measurement depth and a given domain radius. If the available dataset does not fill the simulation domain, the borehole and top or/and bottom layers are expanded to fill the gaps. The code utilizes point-like electrode approximation, therefore exact physical dimensions of the tool and electrodes are neglected. The verticality of the borehole is also assumed in the model. Selected data are passed to the Gmsh where the model is built. At the location of current electrodes, where the greatest variations of electric potential occur, a fine mesh is enforced, while in other parts of the model the mesh is allowed to expand according to constraints dictated by the model geometry. This allows the accuracy of the simulation to be increased while keeping computational cost at a reasonably low level. The model is then passed to NGSolve where a system of equations is assembled and solved. During computations, Lagrange P1 elements are used and a linear system of equations is solved by the conjugate gradient method with a multigrid preconditioner. The result of modelling is the distribution of electric potential within the simulation domain from which values at the location of the measuring electrodes are retrieved and used to calculate the value of the measured apparent resistivity.

RESULTS

The presentation of the results is split into two parts. In the first part, representative modelling results of normal and lateral logs in simple benchmark formation models are presented, where characteristic features of logs are easier to spot. In the second part, two sets of logs utilized in real applications were generated for a more complex formation model. Presented models aim to show how resistivity values measured by different normal and lateral logging tools are affected by the borehole, filtration zone, shoulder beds and dip of the rock formation. However, it should be noted that only a few selected examples are included in the paper. A more detailed and comprehensive discussion of that topic can be found in Serra (1984),

Brock (1986), Jorden & Campbell (1986), Vincent & Williams (1995) and Anderson (2001).

All of the synthetic logs presented in this paper were generated using a default set of parameters chosen for the ReMo3D package. The simulation domain radius was set to 50 m. Generated meshes contained between 9000 and 11,500 elements in the case of 2D models and between 90,000 and 115,000 elements in the case of 3D models. The model parameters necessary to reproduce results are presented in an appendix and the GitHub repository linked at the end of the paper.

Benchmark models

Figure 6 shows synthetic logs generated for a sequence of high resistivity beds of various thicknesses located in a relatively low resistivity background. The borehole diameter is kept at a constant value. A wide range of characteristics typical for normal and lateral resistivity logs crossing high resistivity beds can be seen in the presented examples. Opposite to thin layers tools characterized by shorter spacing measure higher resistivity values than their longer counterparts. An extreme example of that can be seen opposite to the thinnest layer, where in the case of normal tool characterized by longer spacing an apparent resistivity minimum as a result of the thin layer effect can be observed. As the thickness of the layer goes up, the values measured by longer tools exceed the values measured by shorter tools. Observed results are due to a trade-off between vertical resolution and depth of investigation of the tools. Tools with a greater depth of investigation are less affected by the low resistivity borehole mud. However, at the same time, they have lower vertical resolution and are more affected by low resistivity shoulder beds. As expected, normal tools give a symmetric response to layers with the peak value in the middle of the layer (except for the occurrence of an apparent resistivity minimum as a result of the thin layer effect) while lateral tools give an asymmetric response to layers with the peak value near the bottom boundary of the layer in the case of standard tool configuration and near the top boundary in the case of the inverted tool configuration. Features like oil notch, decay zone, shadow zone and reflection peak can also be observed on lateral logs.
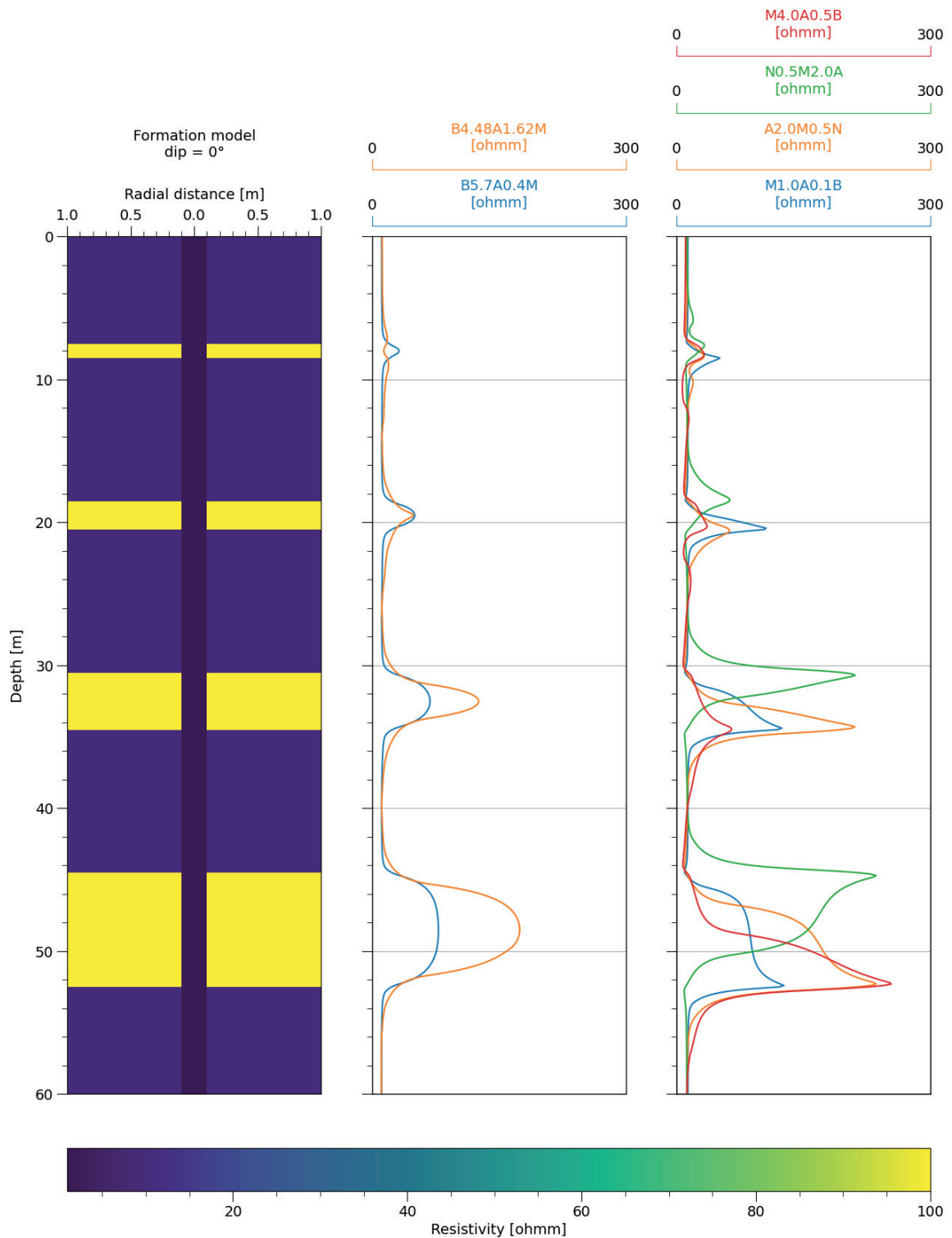
Fig. 6. *Results of modelling for a sequence of high resistivity beds of various thicknesses located in a relatively low resistivity background*

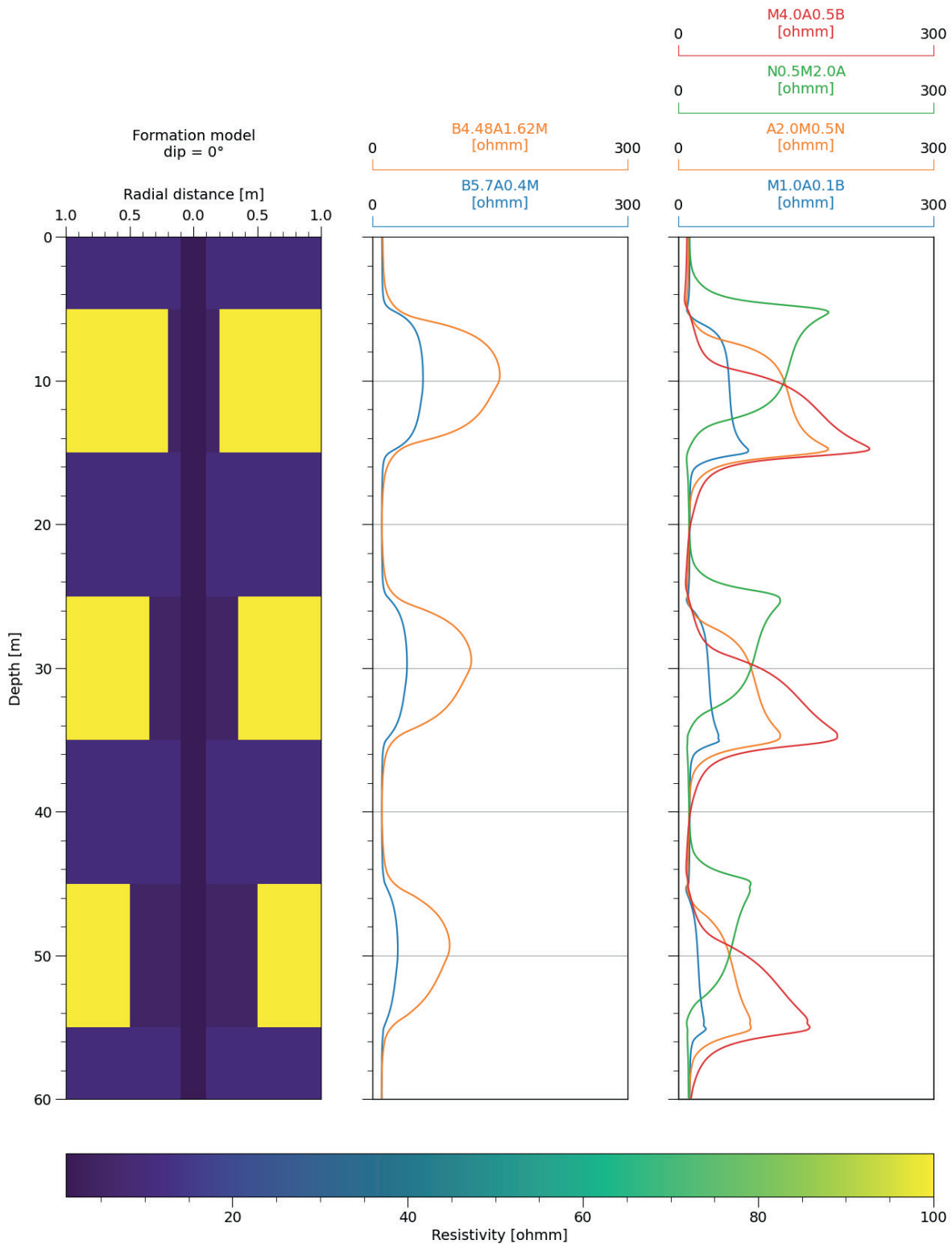Figure 7 shows synthetic logs generated for a sequence of thick high resistivity beds with low resistivity filtration zones of different radii located in a relatively low resistivity background. The borehole diameter is kept at a constant value. Apart from the features described above, the

impact of the filtration zone can be seen on generated data. As expected, logs characterized by shorter spacings are more affected by the presence of the borehole and filtration zone than their longer counterparts and measure lower resistivity values.

Fig. 7. Results of modelling for a sequence of thick high resistivity beds with low resistivity filtration zones of different radii located in a relatively low resistivity background

Figure 8 shows synthetic logs generated for a model containing a single high resistivity layer located in a relatively low resistivity background. The borehole diameter and true thickness of the layer are kept at a constant value. Individual logs were generated for different values of the dip angle of the layer to show how the recorded values of resistivity change with the dip of the layer. The anomaly caused by the high resistivity layer is gradually widening with the increase of the dip angle of the layer. Measured resistivity values are also changing with the dip angle.
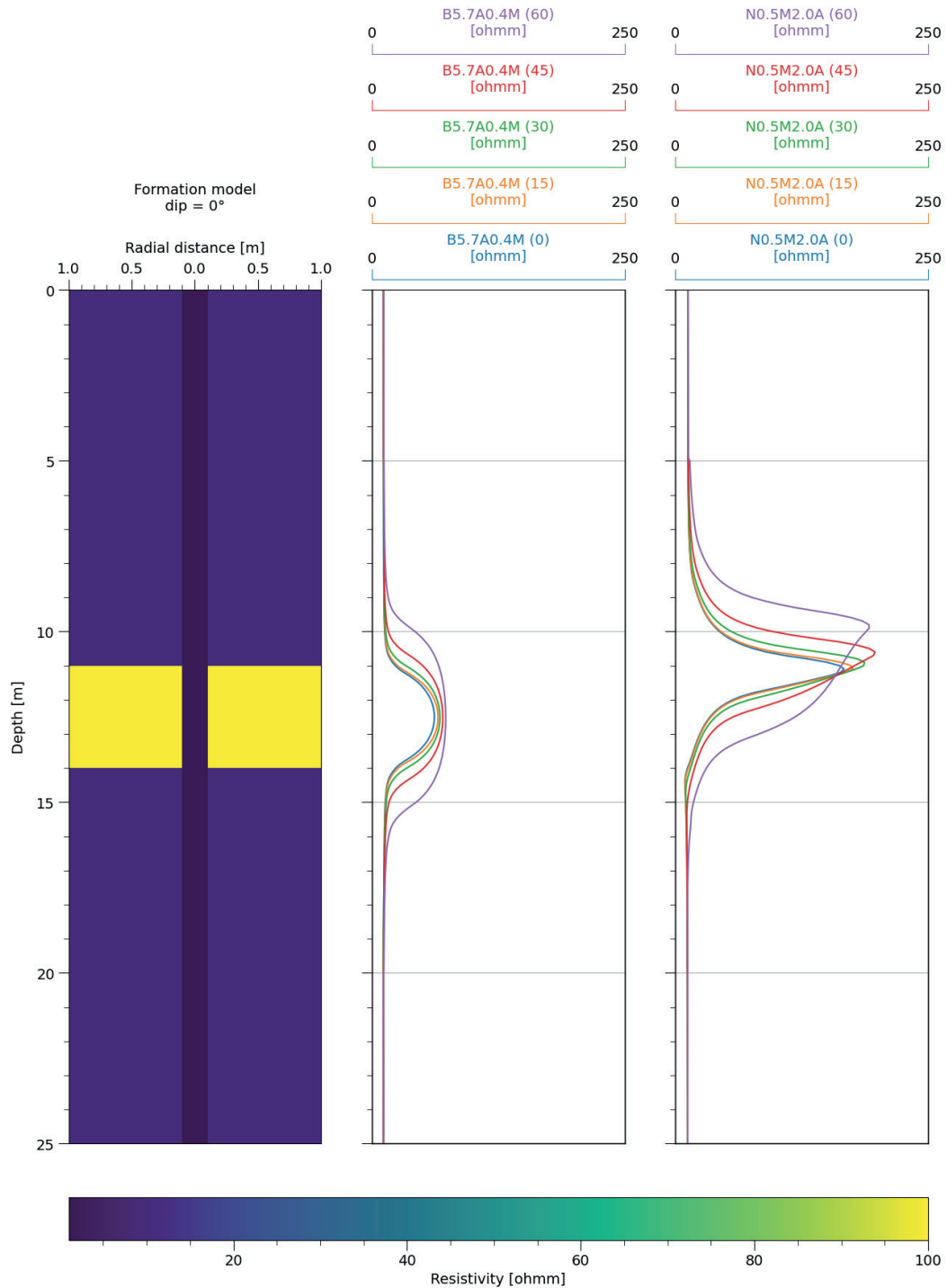
Fig. 8. *Results of modelling for different dip angles (0°, 15°, 30°, 45°, and 60°) of a high resistivity layer located in a relatively low resistivity background*

Complex model

Two sets of logs were selected to show the results of the modelling in a complex model. The first one is a standard suite used in the West – the short normal (16-inch), the long normal (64-inch) and the lateral tool (18 feet 8 inches). The second one represents a suite used in the countries of the Eastern Bloc and comprises five lateral tools characterized by different spacings – M0.5A0.1B, M1.0A0.1B, M2.5A0.25B, M4.0A0.5B, M8.0A1.0B.

Figure 9 shows synthetic logs generated for a complex model with individual layers varying in thickness, resistivities, presence and radius of the filtration zone. The borehole diameter also varies with depth.

The characteristic features of normal and lateral logs are less visible due to the higher complexity of the model, but modelling results reflect interactions between logging tools and different parts of the model well.
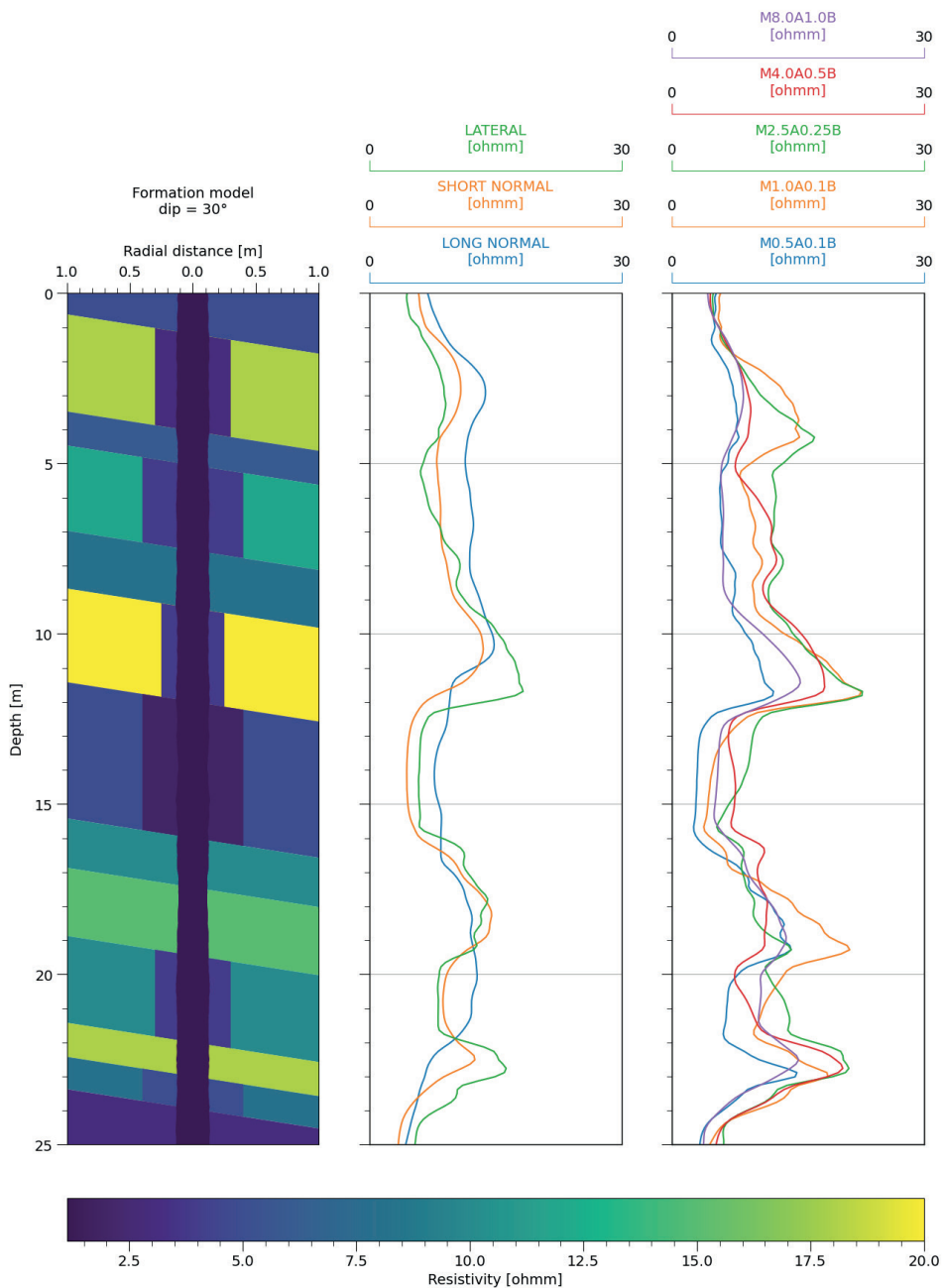

Fig. 9. *Results of modelling for a complex formation model*

DISCUSSION

This paper presented a Python package that allows the generation of synthetic normal and lateral logs for complex 2D and 3D models. The examples included in the paper showed that the software can accurately simulate the physical processes that occur during measurement and produce detailed synthetic logs. The package can be utilized as a standalone modelling tool or as a part of modern interpretation techniques, such as iterative inversion and machine learning. These procedures can address the main concerns related to the utilization of normal and lateral resistivity logs, bringing them closer to modern standards and better suited for utilization in current and future studies. On the other hand, the model geometry utilized within the software is relatively simple. Therefore, the software might be not applicable in the studies where the exact physical dimensions of the logging tool or a more detailed and complex 3D models are necessary (e.g., studies considering layers dipping under various angles and/or with various dip directions, the eccentricity of the logging tool in the borehole or the exact geometry of the borehole).

The code used in this paper is freely available at https://github.com/eMWu94/ReMo3D.

REFERENCES

Acworth I., 2019. *Investigating Groundwater*. CRC Press, London. https://doi.org/10.1201/9781351008525.

Allaud L.A. & Martin M.H., 1977. *Schlumberger: The history of a Technique*. John Wiley & Sons, New York.

Alpin L.M., 1938. *K teorii elektricheskogo karotazha burovykh* skvazhin. ONTINKTIP, Moskva [Альпин Л.М., 1938. *К теории электрического каротажа буровых скважин*. ОНТИНКТIП, Москва].

Anderson B.I., 2001. *Modeling and Inversion Methods for the Interpretation of Resistivity Logging Tool Response*. Delft University Press, Delft [Ph.D. thesis].

Asquith G. & Krygowski D., 2004. *Basic Well Log Analysis*. 2nd ed. American Association of Petroleum Geologists, Tulsa. https://doi.org/10.1306/Mth16823.

Bittar M.S., Shattuck D.P. & Shen L.C., 1995. Finite-element modeling of the normal resistivity tool in azimuthally inhomogenous formations. *Journal of Petroleum Science and Engineering*, 14, 1–2, 59–63. https://doi.org/10.1016/0920-4105(95)00029-1.

Brock J., 1986. *Applied open-hole log analysis*. Gulf Publishing Company, Houston.

Dakhnov V.N., 1941. *Karotazh skvazhin: Interpretatsiya karotazhnykh diagramm*. Gosgeoltekhizdat, Moskva [Дахнов В.Н., 1941. *Каротаж скважин: Интерпретация каротажных диаграмм*. Госгеолтехиздат, *Москва*].

Dalcin L. & Fang Y.-L., 2021. mpi4py: Status update after 12 years of development. *Computing in Science and Engineering*, 23, 4, 47–54. https://doi.org/10.1109/MCSE.2021.3083216.

Dalcin L., Paz R. & Storti M., 2005. MPI for Python. *Journal of Parallel and Distributed Computing*, 65, 9, 1108–1115. https://doi.org/10.1016/J.JPDC.2005.03.010.

Dalcin L., Paz R., Storti M. & D'Elia J., 2008. MPI for Python: Performance improvements and MPI-2 extensions. *Journal of Parallel and Distributed Computing*, 68, 5, 655–662. https://doi.org/10.1016/J.JPDC.2007.09.005.

Dalcin L.D., Paz R.R., Kler P.A. & Cosimo A., 2011. Parallel distributed computing using Python. *Advances in Water Resources*, 34, 9, 1124–1139. https://doi.org/10.1016/J.ADVWATRES.2011.04.013.

Frenkel M.A., 2003. A Model-Based Method to Supply Missing Log Information. [in:] *Proceedings of the AAPG Annual Meeting, Extended Abstracts, Salt Lake City 11–14 May 2003*, 1–7.

Frenkel M.A., Mezzatesta A.G. & Strack K.-M., 1997. Enhanced Interpretation of Russian and Old Electrical Resistivity Logs Using Modeling and Inversion Methods. [in:] *Proceedings, 1997 SPE Annual Technical Conference and Exhibition: 5-8 October 1997, San Antonio, Texas*, SPE-38688-MS, Society of Petroleum Engineers. https://doi.org/10.2118/38688-MS.

Galsa A., Herein M., Drahos D. & Herein A., 2016. Effect of the eccentricity of normal resistivity borehole tools on the current field and resistivity measurement. *Journal of Applied Geophysics*, 134, 281–290. https://doi.org/10.1016/J.JAPPGEO.2016.09.001.

Geuzaine C. & Remacle J.-F., 2009. Gmsh: A 3-D finite element mesh generator with built-in pre- and post-processing facilities. *International Journal for Numerical Methods in Engineering*, 79, 11, 1309–1331. https://doi.org/10.1002/nme.2579.

Glinskikh V., Dudaev A., Nechaev O. & Surodina I., 2017. High-performance computing on GPUs for resistivity logging of oil and gas wells. [in:] *Application of Mathematics in Technical and Natural Sciences: 9th International Conference for Promoting the Application of Mathematics in Technical and Natural Sciences – Amitans '17*, AIP Conference Proceedings, 1895, 120005, AIP Publishing. https://doi.org/10.1063/1.5007422.

Imamura S., 1992. Imaging Technique of Near-Borehole Resistivity Structure From Normal Resistivity Logs. [in:] *Proceedings of the SPWLA 33rd Annual Logging Symposium, Oklahoma City 14–17 June 1992*, SPWLA-1992-F, 1–21.

Imamura S. & Shima H., 1991. Near-borehole Resistivity Imaging Using Normal Resistivity Logs. [in:] *Proceedings of the 1991 SEG Annual Meeting, SEG Technical Program Expanded Abstracts, Houston 10–14 November 1991*, SEG-1991-0145, 145–147. https://doi.org/10.1190/1.1889020.

International Atomic Energy Agency (IAEA), 2001. *Characterization of groundwater flow for near surface disposal facilities*. International Atomic Energy Agency, Vienna.

Jakubowicz W., 1995. Russian well log mnemonics. [in:] Harrison B. (ed.), *Russian-Style Formation Evaluation*, The London Petrophysical Society and The Geological Society London, London, 211–220.

Jorden J.R. & Campbell F.L., 1986. *Well Logging II – Electric and Acoustic Logging*. Society of Petroleum Engineers, New York.

Karataş D.C., Zaman U. & Ulugergerli E.U., 2019. An approach to obtain the structural information from the electrical resistivity well logging curves. *Bulletin of the Mineral Research and Exploration*, 158, 158, 345–352. https://doi.org/10.19111/bulletinofmre.451546.

Keys W.S., 1970. Borehole geophysics as applied to groundwater. [in:] Morley L.W (ed.), *Mining and Groundwater Geophysics, 1967: Proceedings of the Canadian Centennial Conference on Mining and Groundwater Geophysics, Held at Niagara Falls, Canada, in October 1967*, Department of Energy, Mines, and Resources, Ottawa, 598–614.

Keys W.S., 1990. *Borehole geophysics applied to ground-water investigations*. United States Government Printing Office, Washington. https://doi.org/10.3133/twri02E2.

Keys W.S. & MacCary L.M., 1971. *Application of borehole geophysics to water-resources investigations*. United States Government Printing Office, Washington. https://doi.org/10.3133/twri02E1.

Nam M.J., Pardo D., Torres-Verdín C., Hwang S., Park K.G. & Lee C., 2010. Simulation of eccentricity effects on short- and long-normal logging measurements using a Fourier-hp-finite-element method. *Exploration Geophysics*, 41, 1, 118–127. https://doi.org/10.1071/EG09053.

Ogilvy A.A., 1970. Geophysical prospecting for groundwater in the Soviet Union. [in:] Morley L.W (ed.), *Mining and Groundwater Geophysics, 1967: Proceedings of the Canadian Centennial Conference on Mining and Groundwater Geophysics, Held at Niagara Falls, Canada, in October 1967*, Department of Energy, Mines, and Resources, Ottawa, 536–543.

Schöberl J., 1997. NETGEN An advancing front 2D/3D-mesh generator based on abstract rules. *Computing and Visualization in Science*, 1, 41–52. https://doi.org/10.1007/s007910050004.

Schöberl J., 2014. *C++11 Implementation of Finite Elements in NGSolve*. Vienna University of Technology, Vienna.

Serra O., 1984. *Fundamentals of well-log interpretation. 1: The acquisition of logging data*. Elsevier, Amsterdam.

Tingey J.C., Nelson R.J. & Newsham K.F., 1995. Comprehensive Analysis Of Russian Petrophysical Measurements. [in:] *Proceedings of the SPWLA 36th Annual Logging Symposium, Paris 26–29 June 1995*, SPWLA-1995-S, 1–12.

Tittman J., 1986. *Geophysical Well Logging*. Academic Press Inc., Orlando.

Towle G.H., Whitman W.W. & Kim J.-H., 1988. Electric Log Modeling with a Finite Difference Method. *The Log Analyst*, 29, 3, 184–195.

Ulugergerli E.U., 2011. Two dimensional combined inversion of short- and long-normal dc resistivity well log data. *Journal of Applied Geophysics*, 73, 2, 130–138. https://doi.org/10.1016/j.jappgeo.2010.12.004.

Vincent M., Williams F.G., 1995. Unfocused resistivity. [in:] Harrison B. (ed.), *Russian-Style Formation Evaluation*, The London Petrophysical Society and The Geological Society London, London, 129–156.

Whitman W.W., Schön J., Towle G. & Kim J.-H., 1990. An Automatic Inversion of Normal Resistivity Logs. *The Log Analyst*, 31, 1, 10–19.

Whitman W.W., Towle G. & Kim J.-H., 1989. Inversion of Normal and Lateral Well Logs with Borehole Compensation. *The Log Analyst*, 30, 1, 1–11.

Wiltgen N.A., 1994. The Essential of Basic Russian Well Logs and Analysis Techniques. [in:] *Proceedings of the SPWLA 35th Annual Logging Symposium, Tulsa 19–22 June 1994*, SPWLA-1994-II, 1–19.

Wiltgen N.A. & Truman R.B., 1993. Russian Lateral (BKZ) Analysis. [in:] *Proceedings of the SPE Annual Technical Conference and Exhibition, Houston 3–6 October 1993*, SPE-26433-MS, 1–7. https://doi.org/10.2118/26433-MS.

Yang F.-W. & Ward S.H., 1984. Inversion of Borehole Normal Resistivity Logs. *Geophysics*, 49, 9, 1541–1548. https://doi.org/10.1190/1.1441779.

Yang W. & Shi Q., 1999. Apply 2-D Rapid Iterative Inversion for Lateral Resistivity Logs. [in:] *Proceedings of the SPWLA 40th Annual Logging Symposium, Oslo 30 May – 3 June 1999*, SPWLA-1999-CCC, 1–9.

Yuratich M.A. & Meger W.J., 1984. The Application of Finite Difference Methods to Normal Resistivity Logs. [in:] *Proceedings of the SPWLA 25th Annual Logging Symposium, New Orleans 10-13 June 1984*, SPWLA-1984-V, 1–20.

APPENDIX – MODEL PARAMETERS

Parameters of benchmark models presented in the paper are listed below:
– Benchmark model 1 – high resistivity layers of various thicknesses (Figs. A1, A2).
– Benchmark model 2 – high resistivity layers with filtration zones of various radii (Figs. A3, A4).
– Benchmark model 3 – high resistivity layer of constant true thickness and various dip angles (Figs. A5–A10).

DEPT	CALI	RMUD
M	MM	OHMM
0.00	200.00	1.00
60.00	200.00	1.00

Fig. A1. *The borehole model file of the 1st benchmark model*

DTOP	DBTM	RDFZ	RTFZ	RTUZ
M	M	M	OHMM	OHMM
0.00	7.50	NaN	NaN	10.00
7.50	8.50	NaN	NaN	100.00
8.50	18.50	NaN	NaN	10.00
18.50	20.50	NaN	NaN	100.00
20.50	30.50	NaN	NaN	10.00
30.50	34.50	NaN	NaN	100.00
34.50	44.50	NaN	NaN	10.00
44.50	52.50	NaN	NaN	100.00
52.50	60.00	NaN	NaN	10.00

Fig. A2. *The formation model file of the 1st benchmark model*

DEPT	CALI	RMUD
M	MM	OHMM
0.00	200.00	1.00
60.00	200.00	1.00

Fig. A3. *The borehole model file of the 2nd benchmark model*

DTOP	DBTM	RDFZ	RTFZ	RTUZ
M	M	M	OHMM	OHMM
0.00	5.00	NaN	NaN	10.00
5.00	15.00	0.20	5.00	100.00
15.00	25.00	NaN	NaN	10.00
25.00	35.00	0.35	5.00	100.00
35.00	45.00	NaN	NaN	10.00
45.00	55.00	0.50	5.00	100.00
55.00	60.00	NaN	NaN	10.00

Fig. A4. *The formation model file of the 2nd benchmark model*

DEPT	CALI	RMUD
M	MM	OHMM
0.00	200.00	1.00
25.00	200.00	1.00

Fig. A5. *The borehole model file of the 3rd benchmark model*

DTOP	DBTM	RDFZ	RTFZ	RTUZ
M	M	M	OHMM	OHMM
0.00	11.00	NaN	NaN	10.00
11.00	14.00	NaN	NaN	100.00
14.00	25.00	NaN	NaN	10.00

Fig. A6. *The formation model file of the 3rd benchmark model (0° dip)*

DTOP	DBTM	RDFZ	RTFZ	RTUZ
M	M	M	OHMM	OHMM
0.00	10.95	NaN	NaN	10.00
10.95	14.05	NaN	NaN	100.00
14.05	25.00	NaN	NaN	10.00

Fig. A7. *The formation model file of the 3rd benchmark model (15° dip)*

DTOP	DBTM	RDFZ	RTFZ	RTUZ
M	M	M	OHMM	OHMM
0.00	10.77	NaN	NaN	10.00
10.77	14.23	NaN	NaN	100.00
14.23	25.00	NaN	NaN	10.00

Fig. A8. *The formation model file of the 3rd benchmark model (30° dip)*

DTOP	DBTM	RDFZ	RTFZ	RTUZ
M	M	M	OHMM	OHMM
0.00	10.38	NaN	NaN	10.00
10.38	14.62	NaN	NaN	100.00
14.62	25.00	NaN	NaN	10.00

Fig. A9. *The formation model file of the 3rd benchmark model (45° dip)*

DTOP	DBTM	RDFZ	RTFZ	RTUZ
M	M	M	OHMM	OHMM
0.00	9.50	NaN	NaN	10.00
9.50	15.50	NaN	NaN	100.00
15.50	25.00	NaN	NaN	10.00

Fig. A10. *The formation model file of the 3rd benchmark model (60° dip)*